Dominant drivers of Jupiter's H3+ Northern Aurora: 1. magnetic field strength and planetary local time

Stallard, T. S., Knowles, K. L., Melin, H., Wang, R., Thomas, E. M., Moore, L., O'Donoghue, J. ORCID: https://orcid.org/0000-0002-4218-1191, Johnson, R. E., Miller, S. and Coxon, J. C. (2025) Dominant drivers of Jupiter's H3+ Northern Aurora: 1. magnetic field strength and planetary local time. Journal of Geophysical Research: Space Physics, 130 (8). e2025JA034067. ISSN 2169-9402 doi: 10.1029/2025JA034067 Available at https://centaur.reading.ac.uk/124136/

JGR Space Physics

RESEARCH ARTICLE
10.1029/2025JA034067

Dominant Drivers of Jupiter's H_3^+ Northern Aurora: 1. Magnetic Field Strength and Planetary Local Time

Tom S. Stallard[1], Katie L. Knowles[1], Henrik Melin[1], Ruoyan Wang[2], Emma M. Thomas[1], Luke Moore[3], James O'Donoghue[4], Rosie E. Johnson[5], Steve Miller[6], and John C. Coxon[1]

[1]Department of Mathematics, Physics and Electrical Engineering, Northumbria University, Newcastle upon Tyne, UK, [2]School of Physics and Astronomy, University of Leicester, Leicester, UK, [3]Center for Space Physics, Boston University, Boston, MA, USA, [4]Department of Meteorology, University of Reading, Reading, UK, [5]Department of Physics, University of Aberystwyth, Aberystwyth, UK, [6]Department of Physics and Astronomy, University College London, London, UK

Abstract Jupiter's auroral regions are marked by considerable spatial and temporal variability, with numerous sources of auroral enhancements, making it difficult to isolate individual causes of emission brightness. Here, we utilize a data set of >13,000 near-infrared H_3^+ images of Jupiter mapped into latitude, longitude and planetary local time to separate out various sources of emission brightening, smoothed over hundreds of hours of integration and tens of days of observing. We show that H_3^+ equatorial emission is well correlated to planetary local time, indicating that equatorial ionospheric emission is dominated by solar Extreme Ultraviolet (EUV) ionization on the dayside of the planet. H_3^+ main auroral emission is strongly anti-correlated with surface magnetic field strength (with a Pearson correlation of <−0.90), and is also strongly correlated with planetary local time (changing in brightness in the same way as equatorial emission with a Pearson correlation of >0.93). This is the first time such strong correlations have been shown at Jupiter, and may be the first evidence of such direct correlations at any planet, including Earth. Both of these correlations are thought to ultimately result from changes in ionospheric electrical conductivity driven by changing magnetic field strength and solar EUV ionization. This suggests the H_3^+ aurora is significantly controlled by breakdown in co-rotation currents flowing deep into the ionosphere, and that this deep layer contains an important component of solar ionization. However, polar auroral emission does not correlate well with planetary local time, suggesting much more complex processes drive the varying emission within this region.

Plain Language Summary Jupiter's aurora are the brightest in the solar system, glowing in complex patterns that seem to change minute by minute, hour by hour and day by day, making it difficult to understand why these aurora change in brightness as a result of more general trends in the changing conditions at Jupiter. In this work, we combine >13,000 infrared images of the ionosphere, to smooth away the vast range of variations usually seen in individual nights, allowing us to instead reveal two incredibly dominant underlying drivers of infrared auroral brightness. We find that the infrared aurora weakens as the surface magnetic field strength increases, and that the aurora brightens when the ionosphere has been exposed to more ionization from the Sun, so that solar ionization acts as a kind of catalyst, making the aurora brighten far more than the sun can itself ionize. This provides the first clear view of these affects at Jupiter, but perhaps also for the first time at any planet, including Earth. This gives us a potentially universal view of how aurora can change in brightness as the conditions within the ionosphere change.

Key Points:

- Collating >13,000 images has produced the most quintessentially median map of auroral brightness ever made for Jupiter
- Jupiter's main emission is strongly anti-correlated with surface magnetic field strength
- Jupiter's main emission is strongly correlated with planetary local time, strongly enhanced by small scale changes in solar EUV ionization

Supporting Information:

Supporting Information may be found in the online version of this article.

Correspondence to:

T. S. Stallard,
tom.stallard@northumbria.ac.uk

Citation:

Stallard, T. S., Knowles, K. L., Melin, H., Wang, R., Thomas, E. M., Moore, L., et al. (2025). Dominant drivers of Jupiter's H_3^+ northern aurora: 1. Magnetic field strength and planetary local time. *Journal of Geophysical Research: Space Physics*, *130*, e2025JA034067. https://doi.org/10.1029/2025JA034067

Received 10 APR 2025
Accepted 22 JUL 2025

Author Contributions:

Conceptualization: Tom S. Stallard
Data curation: Tom S. Stallard
Formal analysis: Tom S. Stallard
Funding acquisition: Tom S. Stallard
Investigation: Tom S. Stallard, Henrik Melin, Luke Moore, James O'Donoghue, John C. Coxon
Methodology: Tom S. Stallard
Project administration: Tom S. Stallard
Resources: Tom S. Stallard
Software: Tom S. Stallard
Validation: Tom S. Stallard
Visualization: Tom S. Stallard
Writing – original draft: Tom S. Stallard

1. Introduction

Jupiter's aurorae are the brightest and most unceasing in the solar system, and are highly complex in their morphology, dynamics and sources. Jupiter's aurorae are also highly variable and have been shown to change in brightness over a range of different timescales and spatial scales, with these variations occurring alongside a range of conditions within the surrounding space environment, including solar wind strength, Io volcanism and unknown additional effects. This complexity has made it difficult to understand the underlying drivers of auroral emission, resulting in often conflicting views of how individual auroral emission features are produced.

Our understanding of the relative brightness of different regions of the aurora comes from two sources: remote observations from on or close to Earth and in situ measurements made from close to Jupiter. These two sets of observations have revealed the complex nature of Jupiter's aurorae, but are both limited in different ways. Jupiter's aurorae are fixed in jovimagnetic co-ordinates, offset differently from the rotational poles in the northern and

Writing – review & editing: Tom S. Stallard, Katie L. Knowles, Henrik Melin, Ruoyan Wang, Emma M. Thomas, Luke Moore, James O'Donoghue, Rosie E. Johnson, Steve Miller, John C. Coxon

southern hemispheres, positioned such that they rotate into and out of view when observed from Earth. As a result, while Earth-based observations have, over the past three decades, provided a wealth of data exploring the auroral region, these data can only view the aurora from the dayside of the planet, and struggle to resolve emission approaching the planetary limb, limiting views of the aurora close to the rotational pole, especially in the southern hemisphere. In contrast with this, in situ measurements at Jupiter are able to observe the aurora in much sharper detail, but the cadence of such observations are much lower, making each observation a unique and limited case-study view of the aurora.

Although the aurora of Jupiter are contiguous, with numerous individually named features, the complex and interacting auroral emissions are traditionally split into three groups, those originating equatorward of the main emission, the main auroral emission itself and the polar aurorae (Grodent, 2015). In this paper, we focus on the main auroral emissions.

1.1. Main Auroral Drivers

Jupiter's main auroral emission has been studied in detail for more than four decades. The earliest models (e.g., Cowley & Bunce, 2001; Hill, 1979) suggested that this main auroral emission is generated by downward precipitating electrons, accelerated by upward field-aligned currents, produced by the transfer of angular momentum between Jupiter's upper atmosphere and the surrounding magnetosphere.

As magnetospheric plasma moves radially away from the planet, their increasingly slow Keplarian orbits attempt to slow this plasma. This in turn attempts to drag the mapped field lines within the atmosphere and associated ions into sub-corotation. Where this force is relatively weak, the ionospheric ions are forced to move with the surrounding neutrals through collisions, and so both magnetic field lines and magnetospheric plasma are forced to corotate with planet. However, as the plasma moves further from the planet, the required atmospheric torque increases until it overwhelms the atmosphere, and so both the magnetospheric plasma and ionospheric ions begin to sub-corotate.

This azimuthal motion through the magnetic field produces a radial outwards current within the magnetosphere that closes within the ionosphere, driving equatorward Pedersen currents, linked by both upwards and downwards Birkeland currents that flow along the magnetic field lines. It is upwards currents at the equatorward edge of this current system that drives electrons down into the atmosphere, producing Jupiter's bright main auroral emission. These early models, by necessity, considered an azimuthally axisymmetric magnetosphere, but in reality, the magnetosphere is highly asymmetric, resulting in an array of complex auroral features (Bonfond et al., 2020), including some driven by broadband energization (Mauk et al., 2020).

The broad morphology of the aurora is different in the two hemispheres. In the North, the distorted magnetic field results in the main emission following an approximately circular morphology along the westward flank and a highly kinked shape on the east side of the magnetic pole (Connerney et al., 2022; Grodent et al., 2008), while in the south, the aurora sits closer to the pole and has a more circularized morphology (as shown later in Figure 1).

Observations of energetic particles above the dusk auroral region have highlighted two distinct zones of aurora within the main emission, in addition to the diffuse "equatorial" emission described above (Mauk et al., 2020). Zone-I aurora appears to result from active downward electron acceleration, suggesting upward field-aligned currents. This Zone-I aurora appears to align with the narrow, high-color-ratio arc of emission that often dominates within UV emission resulting from enhanced absorption of UV emission at depth (where color ratio is defined as the difference in brightness UV wavelengths relatively unaffected by hydrocarbon absorption divided by the brightness of UV wavelengths strongly absorbed by deep hydrocarbons). Zone-II aurora tends to occur at higher latitudes and consists of bi-directional acceleration of both electrons and protons, with upward fluxes often stronger than downward. The poleward location of Zone-II seems to align it with the fragmented dusk aurora seen most clearly in the H_3^+ aurora. Notably, the dominance of Zone-I and Zone-II aurora appears to change over time, perhaps as a result of the changing dominance of asymmetric magnetospheric currents (Kotsiaros et al., 2019), though these changing in situ conditions have not yet been compared against the changing fragmentation seen within remote Juno imaging (e.g., Greathouse et al., 2021).

The relative brightness of UV and H_3^+ emission are also a significant indicator of precipitation energy. Tao et al. (2011) suggests 10 keV precipitation results in similar brightnesses between UV and H_3^+ emission, with

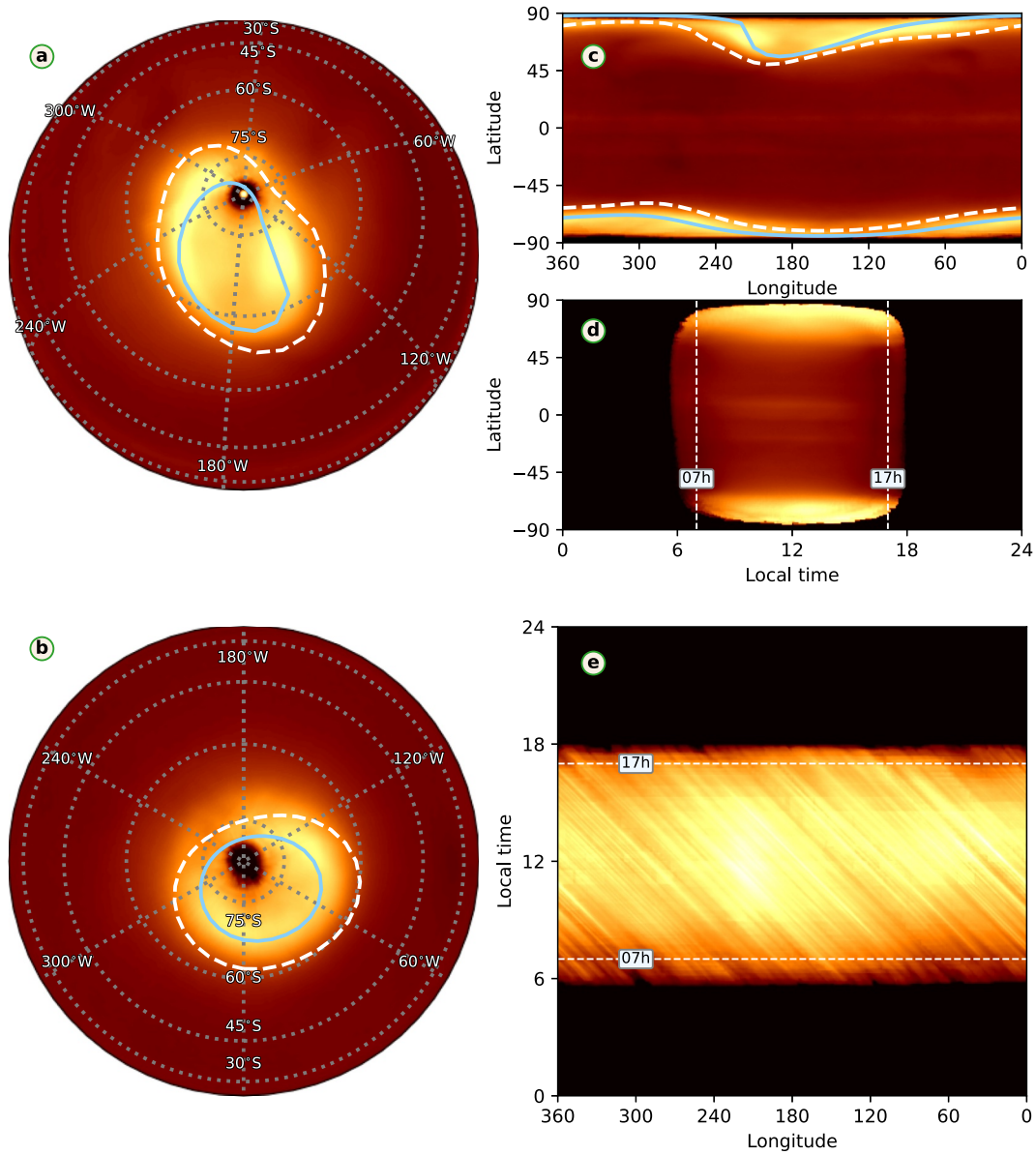

Figure 1. Maps of average emission, across the three dimensions. The average intensity summed across daytime planetary local times between 07:00 and 17:00 is shown in both polar projection (north and south) in panels (a) and (b) respectively, and in cylindrical projection in panel (c). The average intensity summed across all longitudes is shown in panel (d). The average intensity summed across all latitudes is shown in panel (e). All maps are shown with a gamma stretch of 0.5, with a maximum value that best shows the overall emission structure. Panels (a–c) show the location, modeled statistical location of the UV main emission (solid blue) and Io spot (dashed white), taken from Grodent et al. (2008). Panels (d) and (e) shows the range of local times used in this paper, between 07 and 17 hr.

100 keV precipitation producing an order of magnitude more UV than H_3^+ emission, and 0.1 keV precipitation producing an order of magnitude less UV than H_3^+.

This difference between Zone-I and Zone-II aurora has been ascribed to a difference in source, resolved in the differing direction of upwards and downwards currents they are associated with. The narrow Zone-I aurora were associated with deeply penetrating currents that close in the lower ionosphere, driven by the breakdown in co-rotation within Jupiter's middle magnetosphere, previously thought to dominate all jovian main auroral emission (e.g., Cowley & Bunce, 2001), while Zone-II were associated with the downward current region associated

with asymmetric currents closing in the upper atmosphere, with particle acceleration driven by wave-particle interactions, rather than the current system itself (R. Wang et al., 2023).

It is worth noting that these auroral drivers are not mutually exclusive. As much of Jupiter's aurora is due to broadband energization (Mauk et al., 2020) then it can be expected that both hard precipitation (10–100 s keV) and soft precipitation (100 s eV to keV) can be present simultaneously (Damiano et al., 2023). The inertial Alfven wave, in this context, is essentially a wave/particle interaction, but the Alfven wave also carries the field-aligned currents. The extent to which accelerated auroral currents drive regions of Jupiter's main auroral emission remains controversial. Mauk et al. (2017) found that Jupiter's auroral downward energy flux from discrete acceleration is less than that caused by broadband or stochastic processes, but noted that coherent discrete acceleration might trigger instabilities, broadening electron distributions through stochastic processes. Nichols and Cowley (2022) found a clear statistical relationship between the peak auroral UV intensity and longitudinally co-located magnetospheric radial current, compelling evidence that the magnetosphere-ionosphere coupling currents play a key role in powering the main auroral emission. It seems reasonable to assume that regions with predominately downward electrons (i.e., Zone I aurora) are controlled by the influence of Jupiter's breakdown in corotation currents, but that precipitating electrons are produced both through these currents directly and through wave-particle precipitation driven by instabilities resulting from the effects of these currents, so that the originating isolated mono-energetic electron distributions make up only 7% of the final precipitating electron population (Salveter et al., 2022).

No matter the source, the relative brightness of the aurorae are expected to be affected by the strong changes in magnetic field strength at Jupiter, and so will be most strongly affected by the large differences in surface magnetic field strength observed in the north (Connerney et al., 2022).

Plasma is prevented from falling into the atmosphere by stronger magnetic fields, which would result in magnetic field strength and diffuse auroral brightness being inversely proportional, an anticorrelation originally suggested to explain longitudinal variations in images of thermalized infrared emissions from H_3^+ in early work by Connerney et al. (1996).

For discrete aurora at Saturn, equinoctial observations revealed a clear correlation between the calculated magnetic field strength and emission brightness (Nichols et al., 2009), following past modeling by Cowley et al. (2004), argued to result from two identical field-aligned currents in each hemisphere, where the proportional UV emission brightness theoretically scales linearly with magnetic field strength, for a given field-aligned current. This is explicitly stated by Nichols et al. (2009) to contrast directly with diffuse auroral process. This positive correlation between magnetic field strength and auroral brightness was also observed in early spectral observations of H_3^+ auroral emission (Lam, 1996).

However, in discussing these results, Nichols et al. (2009) notes that they assume a similar Pedersen conductivity in each hemisphere and as noted later by Gérard et al. (2013), the Pedersen conductivity can have a significant effect on discrete auroral brightness. The classical expression of Pedersen conductivity σ_P (Evans et al., 1977) highlights the importance of three main components, the electron density n_e, the magnetic field strength B and the relationship between the ion and electron gyrofrequencies, ω_i and ω_e, and ion/neutral collision frequency and total electron collision frequency, ν_{in} and ν_e, respectively:

$$\sigma_P = \frac{en_e}{B}\left\{\sum_i C_i \sum_n \left[\frac{\nu_{in}/\omega_i}{1+\left(\nu_{in}^2/\omega_i^2\right)}\right] + \frac{\nu_e/\omega_e}{1+\left(\nu_e^2/\omega_e^2\right)}\right\} \quad (1)$$

where e is the elementary charge and C_i is the relative ion concentration for a given species. Discussing Saturn's aurora, Gérard et al. (2013) note that, because UV auroral power is directly proportional to the effective Pedersen conductivity and because the Pedersen conductivity is inversely proportional to magnetic field strength, the enhancement modeled in Nichols et al. (2009), should not lead to an enhancement, as these effects balance.

This simplified view of Pedersen conductivity reliance ignores that gyrofrequency ω_i is directly proportional to magnetic field strength. However, the total Pedersen conductivity falls away dramatically in regimes where either $\nu_{in} \gg \omega_i$, deep in the atmosphere where Hall conductivity dominates, or $\omega_i \gg \nu_{in}$, high in the atmosphere, where the lack of collisions nullifies Pedersen conductivity. Close to the Pedersen layer peak, ν_{in}/ω_i approaches 1,

removing any effect from the gyrofrequency dependency. As a result, Gérard et al. (2013)'s inverse correlation is a good approximation, but within the Pedersen layer, the exact magnetic field dependency may vary slightly with altitude.

Follow on modeling of Jupiter by Ray et al. (2014) found that enhanced surface magnetic field strength led to smaller magnetospheric radial currents, as the $J \times B$ force needed to maintain corotation requires a lower current J with enhanced magnetic field strength B. Since these radial currents ultimately close as auroral currents into the atmosphere, this, in turn, results in an inverse proportionality between auroral brightness and surface field strength.

To briefly summarize this array of correlations and anticorrelations between magnetic field strength and auroral brightness:

- for diffuse (broadband) aurora, the brightness should be inversely proportional to magnetic field strength, as particles are more strongly repelled by higher magnetic field strengths
- for discrete (current driven) aurora, the brightness should also be inversely proportional to magnetic field strength, because:
  - auroral brightness is theoretically proportional to magnetic field strength (Nichols et al., 2009);
  - Pedersen conductivity and so, auroral currents and auroral power are inversely proportional to magnetic field strength (Gérard et al., 2013), and;
  - Radial magnetospheric currents and thus auroral power are also inversely proportional to magnetic field strength (Ray et al., 2014).

Notably, Ray et al. (2014) does not include any magnetospheric azimuthal flows in their model. Chané et al. (2013) do not model surface magnetic field strength changes but do model the auroral differences driven by asymmetrical magnetospheric flows. These modeled flows, which are comparable to plasma flows observed by Krupp et al. (2001) and J.-Z. Wang et al. (2024), modulate the breakdown in co-rotation auroral currents, resulting in reduced currents in the noon-dawn sector, as plasma in that region moves much closer to the rotation rate of the planet, while in the dusk-midnight sector, plasma sub-corotates very significantly, enhancing the main auroral emission.

One additional consideration is the effects of changing Pedersen conductivity within the auroral region as a result of varying solar EUV ionization. Jupiter's calculated main auroral conductivity varies a great deal, averaging between 0.5 and 1.0 mho along the main auroral region (Gérard et al., 2020), with this range of conductivities appearing to be dominated by the inverse proportionality to the magnetic field strength. The solar EUV produced conductivity is typically an order of magnitude weaker than this, with the predicted peak solar ionization ranging between 0.06 and 0.2 mho (Tao et al. (2010) and Strobel and Atreya (1983) respectively). However, while these are often smaller in scale than the main auroral conductivity, changes in solar conductance do result in significant enhancement. With a factor of 2.4 enhancement in EUV ionization producing a 30% enhancement in field-aligned currents, Tao et al. (2010) showed a strong noon enhancement in field-aligned currents, weakening toward both dawn and dusk.

Simultaneous auroral observations in both poles are difficult at Jupiter due to the magnetic field offset allowing only one auroral oval to be observed from Earth at any one time. Gérard et al. (2013) made comparisons between conjugate aurora, each observed on the same day as the planet sequentially rotated the north and south aurora into view. These resulted in a range of different brightness ratios between the north and south that do not appear to be well aligned with the respective magnetic field strength, with emission brightness and magnetic field strength appearing to be correlated and anti-correlated on different days, suggesting significant additional sources of auroral enhancement.

Statistical analysis of the UV main emission brightness has shown that the dusk side is a factor of 3 times brighter than the dawn in the south, but only 1.1 times brighter in the north (Bonfond et al., 2015). Since the southern aurora sees notably less magnetic field strength differences than the north, Bonfond et al. (2015) suggest these planetary local time UV brightness differences are driven by a different consequential source, but that this dawn-dusk difference may be attenuated by the effect described in Ray et al. (2014). The main oval also dims markedly near noon (Caldwell et al., 1992), a discontinuity that is present in both hemispheres and confined in magnetospheric local time in the prenoon and early noon sector (Radioti et al., 2008), suggesting a magnetospheric origin for the brightness change, perhaps associated with the dimming predicted by Chané et al. (2013).

Rutala et al. (2024) presented the first large-scale statistical survey of jovian mean UV auroral emission brightness and calculated Pedersen conductivities using more than 200 cumulative hours of HST exposure spanning 2007 and 2016–2019. These were individually mapped into magnetospheric local time and revealed large variations in both northern brightness, calculated auroral currents ($9.34 + 5.72 - 3.54$ MA rad^{-1}) and Pedersen conductivity (0.03–1.66 mho) across all magnetospheric local times. Although the values were highly scattered, they showed a peak in all three values within mapped distances between 20 and 30 R_J and with heightened Pedersen conductivities between magnetospheric local times of 6–9 and 12–13 hr. However, Rutala et al. (2024) only considers the magnetospherically mapped aurora and concludes that, to break the observational degeneracies in their measurements, the data requires analysis under varying ionospheric conductance conditions. As we have discussed above, the most notable ionospheric drivers for conductivity should be changing surface magnetic field strength, which is fixed in system III (i.e., Ray et al., 2014) and the direct changes in conductivity, which will be driven by both magnetospheric processes, but also by EUV ionization within the ionosphere, fixed in planetary local time (i.e., Tao et al., 2010).

As highlighted here, discussions about the effect of local time on auroral brightness are often confused, because of the conflation of two related by notably different forms of local time—within this paper, we distinguish these two forms of local time thus:

1. *planetary local time* denotes the local time within the ionosphere itself, fixed to the Sun as the planet rotates, varying between 0 and 24 hr, where noon (12 hr) faces the Sun. Because of the offset of Jupiter's northern aurora, it is possible for the entire auroral region to be on the dayside in planetary local time (i.e., at planetary local times between 06 and 18 hr);
2. *magnetospheric local time* denotes the local time within the magnetospheric equatorial region that the ionosphere maps to. When the asymmetric northern aurora faces the Earth, the magnetospheric local times are observed in the ionospheric aurora vary broadly like a clock face radiating from the magnetic pole (again, between 0 and 24 hr). However, since magnetic field lines are distorted within the magnetosphere by both the solar wind (bending the magnetic fields approximately antisunward) and internal plasma pressures (bending the magnetic fields approximately sunward), the true mapping is often more complex, and requires detailed modeling to understand (e.g., Vogt et al., 2011).

In conclusion, there are likely to be significant drivers of changing auroral emission strength between dawn and dusk, potentially consisting of both planetary local time difference within the ionosphere itself and those driven by local time differences with the magnetosphere, shaped by magnetospheric morphology and dynamics, but decoupling these two sources of local time difference from each other and from changing magnetic field strength has not been possible with past data sets. In this paper, we focus on the former, how the infrared auroral brightness changes with planetary local time. A later paper will account for the affects discussed here and explore changes with magnetospheric local time.

1.2. Auroral Variability

Jupiter's main aurora has been shown to vary in brightness as a result of changing solar wind conditions (Baron et al., 1996; Clarke et al., 2009), Io activity (Bonfond et al., 2012) and other as yet unknown dynamics (Badman et al., 2016). This long timescale variability makes it difficult to understand the changes in brightness caused by the changing planetary and magnetic local times because of the cadence of auroral images. The cadence is limited by the planet's rotation for remote observations from Earth and limited by spacecraft position for in situ observations at Jupiter. This means that significant changes in emission structure are typically observed on subsequent Earth days (T. S. Stallard et al., 2016).

In addition to this, all regions of Jupiter's aurorae see very significant short-term variability. T. S. Stallard et al. (2016) showed significant standard deviations in the emission brightness across the entire auroral region for all timescales between 2 and 20 min. When viewed as a percentage of total brightness, the largest variations were seen within consistently varying emission in the swirl region and sporadic emission in the active and dusk main emission and appeared weak in the dawn main emission. However, when assessed as an absolute standard deviation, the brightest main auroral emissions were consistently those undergoing the largest changes in brightness. These variations were seen on all time steps explored between ∼2–20 min. While some of these variations are random, quasi-periodic emissions have been identified in multiple wavelengths and timescales. X-ray pulsations

in Jupiter's active region have been associated with UV and radio emission (Elsner et al., 2005), leading to enhancements with periodicities between a few minutes and an hour, with these flares originating from electromagnetic ion cyclotron waves originating within the magnetosphere, seen to vary on the same timescales of emission. Similar pulsations near noon have also been observed in the infrared, again with periodicities in the tens of minutes (Watanabe et al., 2018).

This array of variability, seen on timescales from minutes to days, makes it difficult to separate out the wide range of potential planetary and magnetospheric sources for auroral brightness differences. The ongoing Juno mission promises to gather a wealth of data that will hopefully, ultimately, help resolve some of these questions. Earth-based observations have decades of past measurements that have, recently, been used to collate the first detailed investigation of mean emission brightness with magnetic local time (Rutala et al., 2024). Ground-based H_3^+ observations are similarly deep, providing a wide range of observations, perhaps even less constrained than Hubble in this regard, with observing time only being restricted to periods when Jupiter is available in the night sky. This allows the auroral emissions to be measured across the dayside, a facet utilized by Connerney et al. (1998) to measure the location of the Io spot across all local times in order to produce the VIP4 magnetic model, providing an unprecedented resource with which to understand variations in auroral brightness and morphology on the dayside of the planet, between approximately dawn and dusk. T. S. Stallard et al. (2018) utilized this data set, with careful corrections for aberrant light, to map out the non-auroral ionospheric emission brightness, providing unprecedented views of localized brightening and darkening across the equatorial ionosphere.

Here, we utilize the same data set, adapting the analysis tools used in T. S. Stallard et al. (2018) in order to map the auroral emissions in three dimensions, latitude, longitude and planetary local time.

2. Data Mapping

The data set of observations taken to produce the Connerney et al. (1998) VIP4 model observed Jupiter over a period of 5 years using NASA InfraRed Telescope Facility on Mauna Kea, Hawaii. Over 48 individual observing nights, >13,000 individual images were taken (available at T. Stallard, 2018), with the only strong biases in observational timing being focused on times when Jupiter was close to opposition, and when Io was on the dayside of the planet (so that an Io spot could be observed).

Since the precise filter distributions is not currently available, absolute values for intensity are not available, and so we rely upon the same assumptions presented in T. S. Stallard et al. (2018), to produce a relative H_3^+ emission brightness, given in brightness relative to the average main auroral emission. Using the same processing as T. S. Stallard et al. (2018), we have located the center of the planet for each image, allowing a mapping for each corner of each pixel within each image, accounting for Jupiter's angular diameter, polar flattening, sub-Earth latitude and Jupiter's Central Meridian Longitude, as well as allowing corrections for line-of-sight limb enhancement.

Unlike T. S. Stallard et al. (2018), which mapped individual images into a two dimensional map of latitude and longitude, here, we instead calculate the latitude, longitude and planetary local time, accounting for the angle between Earth, Jupiter and the Sun. Using the values at the four corners, the volume that each pixel fills is then located within a three dimensional data cube of latitude, longitude and planetary local time. As these are summed across the data set, two arrays are produced, one containing the total intensity measured for each pixel and the other containing the total integration time within each pixel, allowing a final mean brightness cube to be produced. Pixels close to the limb of the planet were found to cause significant aberrations in the final maps, and so all pixels within 2% of the limb (measured from the center of the planet) were ignored. A frame-by-frame example of this mapping is shown in Supporting Information S1.

This mapping is completed for every image across all 48 nights of observations outlined in T. S. Stallard et al. (2018), producing two three-dimensional maps of the average total intensity and total integration time across this entire period. As described above, by recording the total intensity and total integration times in two separate arrays, we can combine any range of latitude, longitude or planetary local time, then divide the intensity by the integration time summed across this range to produce an accurate time averaged intensity.

In Figure 1, we show the average H_3^+ emission observed between 1995 and 2000 across these three dimensions, normalized for clarity. First, we combine emission observed across planetary local times between 07 and 17 hr to

produce a map of average intensity in longitude versus latitude. We have projected this map into a northern and southern polar projection (Figures 1a and 1b) and a cylindrical projection (Figure 1c). Second, we combine emission across all longitudes, to produce a normalized cylindrical map of planetary local time versus latitude (Figure 1d). Finally, we combine emission across all latitudes, to produce a normalized cylindrical map of longitude versus planetary local time (Figure 1e).

Of these three maps, only longitude versus latitude (Figures 1a–1c) shows significant structure within the auroral region. These projections are shown with the Grodent et al. (2008) main emission and Io spot locations overlain—these locations were calculated using the peak emission brightness within Hubble ultraviolet auroral images, providing the best direct comparisons between the average UV and H_3^+ aurora. Overall there appears to be a strong correlation between the H_3^+ auroral emissions and their expected location from that model, the northern auroral oval appears slightly poleward of the UV main emission on the left of the map. Although the emission structure is clearer in the northern aurora, partly due to the larger magnetic offset seen in the north, the southern aurora also appears to follow the Grodent et al. (2008) main emission location.

Both the northern and southern polar aurorae exhibit very smoothed out emission structure, suggesting long-term variability. Within the pole, the strong auroral structures identified on both individual images, and on individual days (as highlighted in T. S. Stallard et al., 2016, is smoothed out when averaged over a long time base, observed across a wide range of local times). Equatorial regions hint at the strong ionospheric variations seen in this weak emission, described in detail within T. S. Stallard et al. (2018), but also show horizontal bands of reflected sunlight near the equator, a region that will be ignored in this study, due to the difficulty in removing this equatorial reflected sunlight as it varies with planetary local time. The northern main emission appears relatively uniform across all longitudes, but is notably weaker at its most equatorward extent. Given that this is the region where Jupiter's magnetic field is strongest, this suggests a strong anti-correlation between auroral brightness and the surface magnetic field strength, but further analysis is needed to assess this more fully.

The map of latitude against planetary local time (Figure 1d) shows the broad enhancement of emission at the two auroral poles, but cannot reveal significant structure, since Jupiter's aurorae are fixed in System III longitude. This panel does show an equatorial variation with planetary local time, with a peak emission near noon, as might be expected from H_3^+ generated by solar EUV ionization. Again, reflected sunlight can be seen as bands close to the equator. Notably, however, this planetary local time enhancement appears to continue into the auroral region, suggesting a significant modulation of the auroral brightness with planetary local time—further investigation is needed to resolve whether this is a real correlation, or a trick of summing the data across all longitudes.

The map of longitude against planetary local time (Figure 1e) shows significant broad variability, brightest within longitudes where the northern aurora extends equatorward, and with a clear brightness bias toward noon. The data also contains significant diagonal striations, despite the large number of images used, perhaps the result of individual images showing only auroral or equatorial regions interweaving and overlapping at specific planetary local times. This highlights the need to smooth our datacube over a significant number of either longitude or planetary local time bins to remove this effect. Here, we will smooth over more significant regions of latitude, longitude or planetary local time.

3. Dominant Influences on H_3^+ Auroral Brightness

Having identified magnetic field and planetary local time as two potentially dominant influences on the shape and brightness of both the main auroral emission, we will address each of these in turn, assessing the extent to which these dominate the aurorae.

3.1. Intensity Variation With Total Magnetic Field Strength

In Figure 2, we have plotted how the main auroral brightness is controlled by changing magnetic field strength. As highlighted in the top left panel, we isolate only the main emission for comparison. We constrain the main emission using the Vogt et al. (2011) magnetic mapping, utilizing the updated magnetic mapping from the *JRM09* model (Connerney et al., 2018), the most recently available version of the Vogt et al. (2011) magnetic mapping at the time of this investigation. Using the combined emission from all planetary local times between 07 and 17UT, we exclude any emission mapping into the magnetospheric equator closer to the planet then $R_J < 20$ and further from the planet than $R_J > 80$, to focus on the main auroral emission (based upon predictions by Nichols &

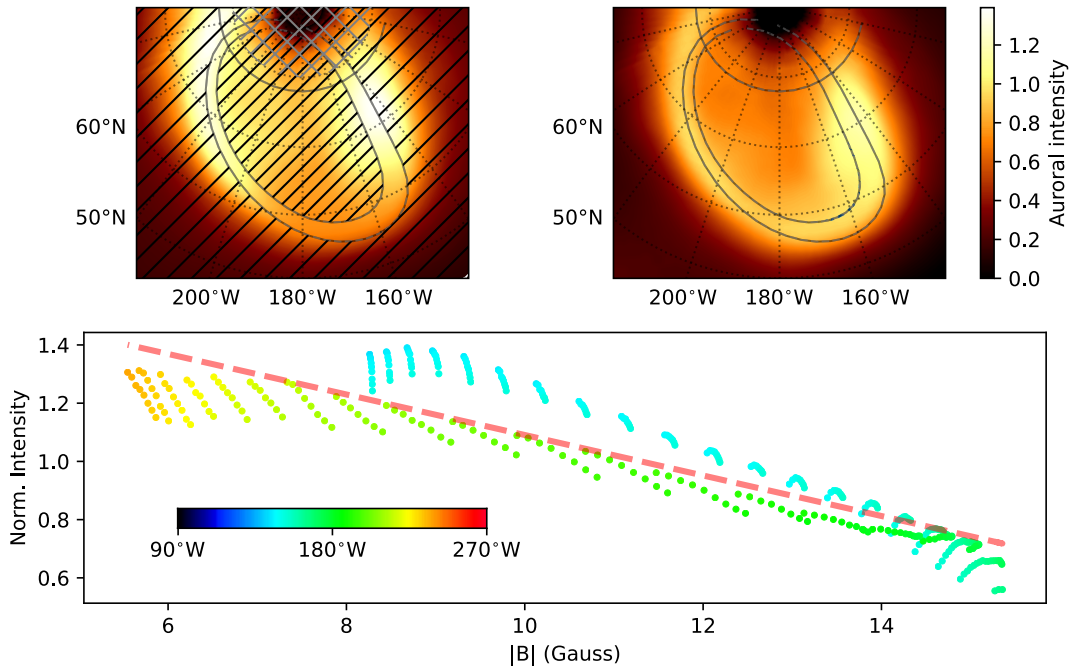

Figure 2. Variation of main emission brightness with magnetic field strength. In the top left panel, the combined emission from planetary local times between 07 and 17 hr is shown, with three regions excluded from comparison (those regions with either diagonal and/or cross-hashed markings). Using the most recent Vogt et al. (2011) magnetic field mapping (that includes the JRM09 Connerney et al. (2018) model), regions mapping closer than $20R_J$ or further than $80R_J$ are excluded (dashed regions). Auroral magnetic mapping represents a CML of 180. Planetary latitudes closer to the pole than 80°N (hashed markings) are also excluded, to avoid the line-of-sight cutout. The bottom panel compares the normalized intensity of the remaining pixels with the co-located calculated total surface magnetic field from the JRM33 Connerney et al. (2022) model, which are then fitted with a linear fit (red dashed). For comparison with the other panels, the west longitude is shown using color, with an inset colorbar as a guide. On the top right panel, the same emission in the other two panels, divided by the fitted correlation between intensity and magnetic field. All intensities are normalized against the mean intensity of the entire selected region.

Cowley, 2004). We also remove emission from close to the rotational pole, to avoid any cut out from line of sight effects. The surface magnetic field strength is then calculated for each pixel using the latitude and longitude of the pixel as an input into the *JRM33* model (Connerney et al., 2022).

Intensities are normalized to the mean brightness of these selected pixels, and plotted against the calculated total surface magnetic field in the bottom panel of Figure 2. There is a clear anti-correlation between emission strength and magnetic field strength, an anti-correlation with a Pearson's correlation of −0.904. The main auroral emission is only 60% of the overall mean main emission where the surface field is strongest (strengthening above 15 Gauss), while the weakest magnetic fields are 120% the overall mean emission. However, it is also clear that, even for the main emission, there are other major controls on emission brightness, with a bimodal distribution of brightness across the two sides of the auroral oval, with one set of values brightening more slowly with field strength (these values come from the more circular part of the auroral region in a longitudinal range of 180–240°W). The second region brightens more quickly with decreasing magnetic field strength, but does not reach as low magnetic field values (coming from the other, more kinked, side of the auroral region at ∼150°W). This contrasted intensity likely originates from the average magnetospheric local times these respective regions map into, which will be discussed in more detail in a later paper.

Overall, the emission brightness approximately doubles with a halving of the surface magnetic field strength. Our linear fit to this data, shown as a dashed line in Figure 2, provides a scaling factor ($\tilde{I} = 1.786 - 0.0675\,|B|$ Gauss) that will be applied to our data set, producing a new normalization for subsequent data. Using the combined planetary local time sectors, the scaled emission brightness is shown in the right hand panel of Figure 2. This results in a much more balanced emission within the main auroral oval, including regions outside our limited

selection, now producing an emission of relatively equal brightness across both polar and equatorial regions with divergent field strengths.

The magnetic field in this region is dominated by the radial surface magnetic field, and there is very little difference between the scaling using total and radial field strength (the later having a Pearson anti-correlation between radial magnetic field strength and main emission brightness of −0.888). The region covered by the polar aurora does not significantly vary in magnetic field strength, and so the morphology is not significantly affected by scaling in this manner.

Assuming this aurora is driven by field-aligned currents from the breakdown in corotation within the magnetosphere, the observed anti-correlation between magnetic field strength and auroral brightness align with the combined predictions of Nichols et al. (2009), Gérard et al. (2013) and Ray et al. (2014), where the respective predicted correlation, anti-correlation and anti-correlation results in an overall anti-correlation with auroral brightness. However, the strong morphological differences between H_3^+ and UV dusk aurora seen by Juno suggest a different precipitating particle energy distribution, and so potentially a different auroral source (Gérard et al., 2018). The Zone-II downward current dominated region observed by Mauk et al. (2020) covers a similar broader region of the H_3^+ aurora, when compared with the Zone-I upward currents associated with deeply penetrating electrons resulting from upwardly directed breakdown in corotation field aligned currents.

If the H_3^+ aurora is primarily generated by wave-particle interactions directly accelerating both ions and electrons into the ionosphere, characteristic of Zone-II aurora, the emission might be expected to be inversely proportional to magnetic field strength, as higher magnetic fields would provide a stronger upward force against this precipitation, though, since the particles are strongly accelerated, this proportionality might be non-linear. It is likely that the H_3^+ aurora is produced through a combination of both auroral currents and wave-particle accelerated aurora.

Gérard et al. (2018) shows images of both H_3^+ and UV emission where the most equatorward aurora (most affected by magnetic field strength) is located in the dawn sector. In this orientation, both the UV and H_3^+ emission appear significantly fainter than at other magnetic longitudes, suggesting the UV emission may be equally affected by magnetic field strength. However, this presents only one case example, and we have previously discussed the stark variability observed at Jupiter—a more rigorous comparison demands a compatible statistical study in the UV.

3.2. Intensity Variation With Planetary Local Time

Figure 3 quantifies the changing emission brightness over different planetary local times, for three different regions: 1) the polar region, 2) the main emission and 3) the non-auroral (equatorial) regions. Given the significant variations seen with magnetic field strength, we first correct our measured emission brightness using the observed magnetic field scaling factor ($\tilde{I} = 1.786 - 0.0675\ |B|$ Gauss). Using this:

1. We constrain the polar aurora by producing an average location of open field lines within the Vogt et al. (2011) model. This provides us with a suitable "polar region" mapping far from the planet, but we note here that the extent of open field lines in Jupiter's polar region is complex, and may include significant regions of closed field lines across the entire polar region (e.g., Delamere et al., 2024; Zhang et al., 2021). Since Vogt et al. (2011) does not provide a specific open field line region, to constrain the open field lines, we take the last closed field line within the model before the fields open, across all modeled planetary local times, and magnetic field mappings. This produces a scattered range of planetary latitude and longitude locations that we fit twice, first with an oval to constrain the center of this region, at 71.54°N and 173.36°W, then with a Gaussian-weighted mean around this fitted magnetic center. This produces an approximation of the open field region highlighted with green text in Figure 3a.
2. We constrain the main emission by using the same main emission region as above, constrained between $20 > R_J > 80$ from the Vogt et al. (2011) magnetic mapping at each planetary local time, taking the median emission within this region, highlighted with blue text. Because we remove data too close in radial distance to the planetary limb, this means noon accesses higher latitudes than near dawn and dusk, and so to balance across all planetary local times, here we exclude all emission poleward of 80°N.
3. To constrain non-auroral emission, we combine light from 15°N to 30°N and 25°S to 40°S, as shown in Figure 3b, highlighted with red text. These asymmetric regions were chosen because they are equatorward

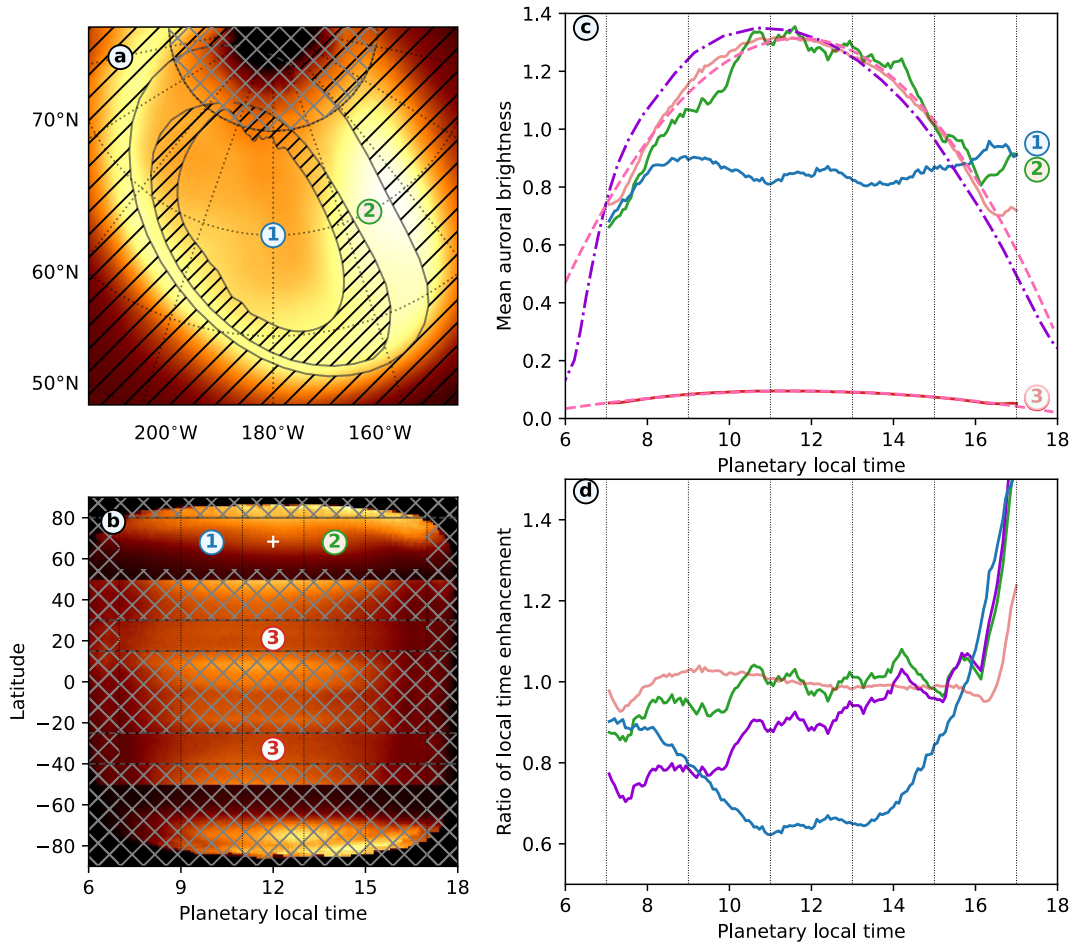

Figure 3. Variation of the auroral brightness with planetary local time. In panels (a) and (b), maps of the three regions used here are shown in latitude-longitude and latitude-planetary local time respectively, using the identical hash markings as in Figure 2. Here, the regions selected are: 1) a region inside the estimated mean open field boundary estimated from the Vogt et al. (2011) model (blue line); 2) the main emission between 20 and 80 R_J, using the Vogt et al. (2011) model (green line); and 3) equatorial emission away from both the aurora and reflected sunlight near the equator (red line), ranging between 15°N–30°N and 25°S–40°S. Auroral magnetic mapping represents a CML of 110. Planetary latitudes >80°N are also excluded, as above. In panel (c), we show the median emission brightness within each delineated region, calculated for each planetary local time slice between 7 and 17 hr in steps of 4 min. The non-auroral emission must be scaled up by 13.82 (pink solid line) to match with the brightness of the main auroral emission, and is fitted with a second order polynomial (pink dashed line). For comparison, we also show the predicted variation in auroral brightness predicted by Tao et al. (2010), scaled to the peak brightness of the main auroral emission (purple). In panel (d), we show the ratio of each of the three regions (again in blue, green and pink) against the scaled, fitted equatorial emission (in dashed pink line in panel c), as well as the ratio of the main auroral emission against the predicted brightness from the Tao et al. (2010) model (purple).

enough to avoid auroral contamination, either from direct precipitation or emission enhancement from enhanced temperatures, but poleward of the equatorial region in which significant reflected sunlight distorts the emission map, both discussed in detail within T. S. Stallard et al. (2018) (NB: this region is too equatorward to appear in Figure 3a).

Both magnetic mapping of the open field line region and main emission are recalculated for each planetary local time, since these change as the planet rotates, so that the auroral binning matches. Figure 3a shows the magnetic mapping at a CML of 110, while the top panels in Figure 2 use a CML of 180.

For each of these three regions, we find the median brightness with the region for individual slices of planetary local time, with the slice width being a single degree of local time (i.e., a planetary local time width of 24 hr/360°, or 4 min). These measured median brightnesses were measured between planetary local times of 07 and 17 hr, and are shown in Figure 3c, as 1) blue, 2) green and 3) red lines respectively.

In order to compare our auroral emissions with the observed and modeled enhancements from the EUV ionization, we also provide scaled versions of these values. To highlight the observed variation in equatorial emission, we scale this emission to the peak auroral brightness (shown as a pink line in Figure 3c), and fit the equatorial emission with a second-order polynomial (with the fitted values of -7.176×10^{-6}, 1.9448×10^{-6} and -8.3156×10^{-8}), which is also scaled to the peak brightness (shown as a dashed pink line in Figure 3c). To compare with the predictions of Tao et al. (2010), we have also scaled their predicted latitudinally averaged field aligned currents to our peak auroral brightness, the purple dot-dash line in Figure 3c.

To further compare these values, in Figure 3d we divide the three observed regions by the fitted and scaled equatorial emission (the dashed pink line in Figure 3c). This highlights that the equatorial emission (pink line), as might be expected, matches well with the polynomial fit to that emission. Notably, the main auroral emission (blue line) also matches very well across most planetary local times, while polar aurora (green line) do not match well at all. We also compare the main auroral emission with the distribution predicted by Tao et al. (2010) by dividing the main emission brightness by the scaled values for that model (purple line).

Past modeling (e.g., Achilleos et al., 1998) has shown that the non-auroral emission is strongly controlled by EUV ionization, with lifetimes short enough that this results in a peak ionization close to the sub-solar point, resulting in an enhancement at the planetary noon meridian (in contrast with H^+ density at Jupiter and H_3^+ density at Uranus, where the ionosphere has an extended lifetime that enhances emission on the dusk side, e.g., Melin et al. (2019)). Here, the equatorial H_3^+ emission peaks slightly before noon and falls away relatively symmetrically on each side. The buildup of H^+ between dawn and dusk (Achilleos et al., 1998) is predicted to drive a slightly duskward bulge in the equatorial H_3^+ density. While any dawnside offset is most likely the result of noise in our measurements, the lack of a significant duskward extension does confirm a relatively short lifetime for H_3^+, even within the equatorial regions, and the close symmetry between dawn and dusk suggests limited production of H_3^+ from H^+ in these equatorial regions, perhaps providing future constraints on models of the $H^+ + H_2^*$ reaction rate.

The main auroral emission is very strongly correlated with this same EUV enhancement—the median brightness within the two regions have a Pearson's correlation of 0.936, indicating that both the auroral and non-auroral H_3^+ emission at Jupiter is very strongly controlled by the extent of solar EUV ionization. However, the scale of the auroral enhancement is much larger than can be explained by the enhancement of background H_3^+ through solar ionization. To highlight the correlation between planetary local time equatorial enhancement and auroral brightness, Figure 3c not only plots the two regions of auroral emission alongside both the equatorial emission normalized in the same way, but also scales up the equatorial emission by a factor of 13.82 to match with the mean auroral brightness. This suggests less than 10% of the auroral enhancement comes directly from increased H_3^+ density from solar EUV enhancement. While this enhancement is likely to be in part the result of the higher auroral temperatures within the auroral region, the auroral region is also at least an order of magnitude more dense (e.g., Moore et al., 2017). This suggests that auroral production of H_3^+ is likely enhanced by the increased conductivity associated with solar EUV, allowing much stronger auroral precipitation to flow near noon than dawn or dusk.

Past estimations of Pedersen conductivity from Juno measurements aligned the conductivity strongly with H_3^+ density (Gérard et al., 2020), suggesting aurorally generated ions are the primary source of Pedersen conductivity (with H_3^+ and hydrocarbons contributing approximately 50% each). However, while Gérard et al. (2020) compare the hemispheric differences in Pedersen conductivity, they do not account for local-time changes. As Tao et al. (2010) highlighted, the solar EUV acts to enhance overall Pedersen conductivity, allowing more rotational energy to couple into the ionosphere.

The close alignment between the main auroral emission and the prediction of auroral brightness from Tao et al. (2010), highlights how well the Tao et al. (2010) model predicted the changing auroral brightness with planetary local time on the dayside, with a Pearson correlation between the scaled modeled brightness and measured emission of 0.803. The main offset between Tao et al. (2010)'s auroral brightness and those observed here are the result of Tao et al. (2010)'s inclusion of the changing magnetospheric plasma densities with "local time"—essentially, their model blends the ionospheric conductivity observed in planetary local time with the magnetospheric plasma density in magnetospheric local time. The dawnward shift observed in Tao et al. (2010) becomes more asymmetric with increasing assumed plasma densities. Having observed across a wide range of magnetospheric local time in each planetary local time bin (because of the deformation of magnetic field lines

between the planet's surface and the magnetospheric equator), all but the strongest asymmetries should be blended out.

However, we note that Tao et al. (2010) predicts up to two orders of magnitude weaker emission on the nightside of the planet, but Juno observations have shown that the nightside H_3^+ emission remains comparably bright, with no clear day-night shift in overall brightness (Gérard et al., 2018). This may suggest that at a base level, the aurora is self-sustaining, with auroral currents sustaining Pedersen conductivity in the auroral region, preventing a collapse of the nightside auroral ionosphere. Above this base line, H_3^+ emission is increased by a scaled enhancement from the EUV ionization on the dayside. A more detailed statistical comparison using Juno UV data (which includes nightside emission) would help understand this correlation better.

Importantly, given that wave-particle driven auroral precipitations are unlikely to be significantly enhanced by Pedersen conductivity, this suggests that H_3^+ auroral brightness is strongly correlated with field-aligned currents and particle precipitation, and that the Zone-II aurora observed above the planet (Mauk et al., 2020) are at least partially controlled by bi-directional, downward dominated, field-aligned current systems.

Although very well correlated, Tao et al. (2010) predicts a dawnward shift in the peak auroral emission, something not observed in this data. The main emission is instead clearly enhanced at dusk, compared with relatively weak emission in dawn. This could indicate a source of enhanced precipitation at dusk (as predicted by Bonfond et al., 2015), weakened auroral currents at dawn (as predicted by Chané et al., 2013) or a combination of both effects. We will explore the magnetospheric context of these variations in brightness in a later paper.

In contrast with the main auroral emission, Jupiter's "open" polar region (as defined by Vogt et al., 2011, though potentially significantly closed) appears largely independent of the non-auroral solar-EUV enhanced emission. The emission appears somewhat enhanced at dawn, dusk and noon, and slightly reduced close to 11 and 13 hr, but these variations are relatively small. This strongly suggests that the average auroral brightness in the polar region varies in a non-linear way with planetary local time, and is not dominated by the influenced of the background conductivity as is the main emission.

This is particularly noteworthy, because Juno measurements of the nightside UV aurora have shown clear emission from the main auroral emission across all planetary local times, and yet the polar aurora is far weaker on the night side, though not always entirely extinguished (Greathouse et al., 2021). Comparable reductions in the H_3^+ auroral brightness are also not readily apparent when these polar aurorae are compared (Gérard et al., 2018). It is possible that there is a threshold of minimum ionization above which the polar auroral processes are indifferent to changing conductivity, but the broader collapse of the ionosphere on the non-illuminated nightside greatly weakens the polar emission. The highly variable nature of polar emission may make it harder to sustain into the nightside, resulting in it extinguishing in a way not seen within the main emission. Alternatively, the strong dayside planetary local time dependence of the polar aurora might continue onto the nightside, with the significantly weaker UV emission associated more with magnetic field line direction than Pedersen conductivity alone.

Most notably, this strong polar variation highlights the need for more detailed investigation of what is driving these changes in emission with planetary local time, something that will be investigated in detail in a later paper.

The final panel of Figure 3 shows the brightness of the main auroral emission and polar emission divided by the scaled, fitted equatorial emission (in dashed pink line in panel c). Here, the auroral emission is close to flat, with a slight slope in enhancement from dawn to dusk (blue). As we will see later, there is a significant enhancement in regions mapping to the magnetospheric dusk region, which, since we are observing from Earth, are biased toward planetary dusk. The polar regions are moderately enhanced in the dawn region and very strongly enhanced in the dusk region, indicating a potential spike in emission in these regions, though equally, the processes driving emission in these regions might be independent of the equatorial emission. All three sources of emission show similar sharp enhancement close to dusk, most likely indicating limitations with the data in this extreme planetary local time. The ratio of main emission brightness against the predicted auroral enhancement from Tao et al. (2010) are strongly pre-noon weak and post-non enhanced, again because of the confluence of magnetospheric local time dominated magnetospheric plasma density within that model, that are smoothed out here.

4. Comparisons With Past UV Observations

We have confirmed, for the first time, two very strong drivers of Jupiter's H_3^+ emission brightness, with an anti-correlation with magnetic field strength and correlation with planetary local time, both likely resulting from enhancements in the local Pedersen conductivity, not previously measured in past studies.

This study might be argued to be of somewhat limited utility in understanding the underlying drivers of brightness differences within the UV H and H_2 emission. First, H_3^+ is strongly modulated by temperature, which in our brightness measurements are intractably coupled to the density. A more detailed study of individually measured temperatures and densities would be the only way to fully separate these components of the H_3^+ brightness, with H_3^+ density being a far stronger proxy for the UV emission (since UV H_2 emission is produced by excitation processes that fail to fully remove the electron from the molecular hydrogen, while the former is primarily produced from molecular hydrogen where the electron was stripped from the molecule).

However, even with this closer proxy, H_3^+ emission provides only an approximation for any UV emission, since the brightness of each is modulated differently for different mean precipitation energy and energy flux. These are equally difficult to disentangle from our H_3^+ brightness measurements, but will have important effects on any perceived magnetic field or Pedersen conductivity correspondences with brightness.

4.1. Very High Precipitation Energies

For the case where the mean precipitation particle energy is very large, most of the ionization will penetrate deep into the atmosphere, deposited below the Pedersen layer. In this case, the component of H_3^+ emission observed might represent only the upper-most ionospheric layer, and miss the majority of precipitation that falls much deeper, since H_3^+ is quickly destroyed deeper in the atmosphere.

- One potential conclusion from this is that UV emission to arise from deeper in the atmosphere, in a layer dominated by Hall currents. This would be beneath the region where Pedersen currents effectively close the currents, and so UV emission might not have an associated strong correlation to the Pedersen conductivity.
- Despite this, it is broadly agreed that the primary driver of the main auroral emission is upward currents driven by the breakdown of co-rotation currents (e.g., Gérard et al., 2013; Nichols et al., 2009; Ray et al., 2014). These currents must close in the ionosphere. However, it is not true that they must close through the Pedersen layer. It is often said that field-aligned currents must close through Pedersen currents due to the work of Fukushima (1976), but this assumes the Hall conductivity is uniform. As exploited in the Spherical Elementary Current System technique (Amm, 1997; Amm & Viljanen, 1999), in the case of non-uniform conductivity the Hall layer plays a part in the current closure. This has been exploited to measure field-aligned currents from the ground at Earth (e.g., Juusola et al., 2023; Oliveira et al., 2024; Weygand et al., 2023 and references therein).
- Without a fuller understanding of how Jupiter's currents close within the extended layers of the ionosphere, it is thus possible that especially high color-ratio UV emission is driven by different ionospheric conductivity than govern the H_3^+ auroral brightness, and will see differing variations with planetary local time.

4.2. Low Precipitation Energies

For the case where the mean precipitation particle energy is small, then the majority of ionization will occur high in the ionosphere, and H_3^+ emission will be enhanced while contributing only very slightly to the overall UV emission. Models of H_3^+ emission show that it is confined to a limited range of altitudes, as very high ($> 2{,}000$ km) emission will be reduced by the breakdown on local thermal equilibrium, and below the homopause H_3^+ is quickly destroyed (Tao et al., 2011). However, this emission would occur well above the Pedersen layer and could not be driven by the breakdown in corotation currents that typically close deep into the atmosphere (Tao et al., 2009).

- As such, if the aurora originates high in the ionosphere explaining the strong correlation between brightness and planetary local time is difficult, since this correlation can no longer originate from Pedersen conductivity.
- What is clear, however, is that enhancement is fixed in planetary local time, rather than magnetospheric local time. The solar wind bends-back magnetic field lines toward midnight very differently as the offset northern auroral region rotates from dawn to dusk (Vogt et al., 2011), so that magnetospheric and planetary local time are poorly aligned within the ionosphere. For instance, the main auroral brightness at a planetary local time of

noon, as shown in Figure 3, includes measurements that map to magnetospheric local times between ∼04–20 hr. We will explore the variations in emission brightness with changing magnetospheric local time in more detail in a later paper.

4.3. Breakdown in Co-Rotation Closing Currents

Recent observations of the "effective ion drift" associated with Pedersen currents that close within the H_3^+ dense region of the ionosphere highlight that corotation currents do not close within these regions (R. Wang et al., 2023). Instead, this region is dominated by Pedersen currents associated with asymmetric magnetospheric flows dominated by the cross-tail current, similar to the dominant ion winds observed at Earth. That paper suggests that H_3^+ emission is produced by a combination of a narrow arc of emission produced by downward accelerated electrons produced by breakdown in co-rotation aurora closing deeper in the ionosphere, and a wider region of aurora produced by electrons accelerated by wave-particle interactions that happen to precipitate into the ionosphere in a region of downward current, and closes in the upper ionosphere where H_3^+ dominates. This downward current might accelerate protons into the planet to produce the aurora observed in this region, but the lack of a matching accelerated electron aurora where the current is upwards suggests this is unlikely.

- The strong correlation between Pedersen conductivity and main emission brightness cannot originate solely from emission driven by wave-particle interactions since wave-particle interactions are largely independent of ionospheric conditions, and, as discussed above, cannot originate from currents closing within the H_3^+ emission layer. This strongly suggests that a significant proportion of H_3^+ auroral emission originates from the same breakdown in co-rotation driver that also dominates the UV auroral emission.
- This, in turn, strongly suggests that UV emission is likely also strongly modulated by planetary local time and that solar ionization likely penetrates relatively deeply into Jupiter's ionosphere, allowing the deep layers where breakdown in co-rotation currents close to be affected by changing solar illumination.
- However, since wave-particle interactions in the magnetosphere are independent of the ionospheric Pedersen conductivity, a combination of both breakdown-current particle precipitation and wave-particle interaction acceleration aurora would still show a strong correlation between Pedersen currents and total auroral brightness, if these other drivers of variations are sufficiently smoothed over the averaged intensity. As such, we cannot use the strong planetary local time correlation to decouple H_3^+ emission from wave-particle-interaction-driven particle precipitation not associated with instabilities produced by breakdown in corotation currents.

4.4. UV Swirl Region Emissions

Finally, while these arguments hold to some degree within the main auroral emission and, perhaps, the Active and Dark polar regions, they breakdown completely within the Swirl region, because this region has very high color ratio UV emission that appears to be driven from relatively low flux but very high precipitating energy particles deep in the ionosphere, well beneath the homopause. Within the main auroral emission, localized bright spots in UV emission that are associated with high energy particles with high flux typically fail to strongly enhance H_3^+ emission (T. S. Stallard et al., 2016). Since the infrared polar regions are often strongly associated with relatively bright H_3^+ emissions, this presents an apparent contradiction.

- One resolution for this might be that the H_3^+ emissions is enhanced by increased temperatures over the pole, though past measurements have suggested only moderate changes ($\lesssim$10%) over this region (e.g., Johnson et al., 2018; Moore et al., 2017; T. Stallard et al., 2002).
- Recent measurements of Jupiter's mid-infrared emissions from the auroral region suggest the homopause altitude increases from ∼360 to ∼460 km inside the main auroral region, driven by auroral heating within the stratosphere (Rodríguez-Ovalle et al., 2024; Sinclair et al., 2020), compared with an auroral H_3^+ emission peak close to 650 km (Kita et al., 2018). It may be that high-color ratio UV emissions in the pole are not caused by high-energy particles, but instead represent lower energy particles that mirror deeper across the pole because the atmosphere is distorted by the extended homopause.
- Alternatively, the varying neutral dynamics observed to change with altitude within the auroral regions, fastest in the upper ionosphere (R. Wang et al., 2023), slower in the upper stratosphere (Cavalié et al., 2021) and slower still in the mid-stratosphere (Tsubota et al., 2024) might also cause significant differences in the polar atmosphere.

As such, while the UV main auroral emissions are more strongly driven by breakdown-in-corotation currents, and the H_3^+ main aurora more strongly by wave-particle interaction driven precipitation, there is a significant overlap between these aurora in terms of both morphology and source, and so our observations here do provide significant information about the varying controls on both H_3^+ and UV main auroral emission, especially with low color-ratio UV emissions.

5. Conclusions

This investigation has revealed two very strong controls on the H_3^+ emission brightness within the northern auroral region:

1. The H_3^+ main auroral emission is clearly highly controlled by the surface magnetic field strength, with an anti-correlation of better than −0.90, and with emission brightness doubling with a halving of the total magnetic field strength. This compares well with the previously observed differences in UV emission brightness between the northern and southern aurora, with the factor of three enhancement in the southern aurora previously ascribed to the much weaker field strength seen there. Here, we confirm that association, and show that the anti-correlation is approximately linear within the main emission.
   (a) If the H_3^+ emission is driven by co-rotation breakdown currents, this could confirm the prediction of Ray et al. (2014) that field-aligned currents are anti-correlated with magnetic field strength, as currents are balanced against field strength within the required $\mathbf{J} \times \mathbf{B}$ force needed to maintain corotation in the magnetosphere;
   (b) Alternatively, however, if the H_3^+ emission is driven by wave-particle interactions within the magnetosphere, accelerated electrons and ions would be preferentially prevented from precipitating into the atmosphere by higher magnetic fields, and so such aurora would also be strongly anti-correlated with the magnetic field strength.
2. The H_3^+ main auroral emission is also strongly controlled by planetary local time, with a correlation between the main auroral emission and equatorial emission (which in turn is strongly modulated by planetary local time) of better than 0.93 once the magnetic field strength dependency is accounted for, suggesting that the enhancement in conductivity from EUV ionization may be a significant contributing factor in the main emission brightness.
   (a) This implies a significant contribution to H_3^+ emission from field-aligned currents, which are directly proportional to Pedersen conductivity, rather than precipitation driven by wave-particle interactions, which should be relatively independent of ionospheric conditions.
   (b) The correlation between H_3^+ emission and the Zone-II aurora observed by Mauk et al. (2020) has previously been associated with wave-particle interactions rather than downward currents (R. Wang et al., 2023). This suggests these emission, while significant in brightness, do not bias the apparent strength of correlation with planetary local time, perhaps indicating this correlation is even stronger within the Zone-I aurora driven from depth.
   (c) This, in turn, suggests the deep Pedersen layer in which breakdown in co-rotation currents close is strongly enhanced by solar EUV ionization.
3. The H_3^+ polar emission is poorly correlated with planetary local time, in contrast with both the main auroral emission and non-auroral emission. This suggests more complex processes are driving changes in polar morphology with changing planetary local time, perhaps driven by changes in the precipitation energy, which will be explored in more detail in a later paper.

These results sit in the context of our knowledge of field-aligned currents flowing at Earth. Coxon et al. (2016) discovered an asymmetry between the field-aligned currents in the Northern and Southern Hemispheres, later confirmed by subsequent observations (Coxon et al., 2022; Workayehu et al., 2019, 2020, 2021; Xiong et al., 2020). Laundal et al. (2016) et al. suggested that this might be driven by asymmetries in Earth's internal field, but this has not been explicitly tested. The results seen here, demonstrating that stronger aurora are seen in regions of lower magnetic field, are potentially consistent with the Coxon et al. (2016) observations as Earth's Northern Hemisphere has overall weaker magnetic field than the Southern Hemisphere. To our knowledge, nobody has reported observations of a long-term statistical hemispheric asymmetry in Earth's aurora, but the present study hints that such a study would be instructive. In return, studies of ionospheric current at Earth

(e.g., Juusola et al., 2023; Weygand et al., 2023) indicate that the observations herein can be partly explained by the fact that the Hall layer is also important for current closure.

Ultimately, this study benefits from an incredible observational data set with a highly sampled long temporal sequence. These data, when averaged over the entire data set, provide a uniquely smooth view of Jupiter's highly complex aurora and allowing us to identify the broadest controls on emission. It reveals a main emission that is strongly controlled by planetary local time, and inversely controlled by the surface magnetic field strength. One follow-up to the work in this paper will be to explore this data set more deeply, and map emissions out into the surrounding magnetosphere, in a similar way to Rutala et al. (2024). Both this data set and that of Rutala et al. (2024) would benefit greatly from accounting for magnetic field strength and planetary local time before mapping out into the magnetosphere, as these affected, fixed in position within the ionosphere, are scattered across a wide range of magnetospheric local times and would appear within uncorrected mapped values as random noise.

However, both these data sets are also limited in their ability to reveal detail. Ground-based measurements are limited in their spatial accuracy, and all Earth-based observations can only provide a view of the auroral region across less than half of all planetary local times. Fortunately, as the Juno mission continues to take observations of Jupiter's aurora at incredible spatial scales and a wide range of planetary local times, it is likely that the number of images taken will soon become dense enough to provide clear statistical averages for changing latitude, longitude, planetary and magnetospheric local times and potentially even for changing magnetospheric driving (e.g., from changing solar wind conditions). As a result, maps of varying auroral emission brightness and UV spectral color at much higher levels of detail will become viable. These promise to reveal far more than this preliminary study was able to, and may represent a profound shift in our understanding of auroral processes at Jupiter.

Inclusion in Global Research Statement

A clear understanding was reached among collaborators with regard to their roles, responsibilities and conduct throughout the research cycle, from study design through to study implementation, review and dissemination.

Data Availability Statement

The images used in this publication is available from Stallard (2018). The code and processed data cube used to produce the figures in this paper are available from Stallard (2025).

Acknowledgments
T.S.S. and E.M.T. were supported by the STFC Consolidated Grant (ST/W00089X/1). H.M. was supported by the STFC James Webb Fellowship (ST/W001527/2). L.M. acknowledges support from Program number JWST-GO-05308.001-A provided through a grant from the Space Telescope Science Institute under NASA contract NAS5-03127. J.O'D. was supported by the STFC Ernest Rutherford Fellowship (ST/X003426/1). K.L.K. was supported by a Northumbria University Research Studentship. J.C.C. was supported by the STFC Ernest Rutherford Fellowship (ST/V004883/1). Data were provided by the Magnetospheres of the Outer Planets Infrared Data Archive, Laboratory for Atmospheric and Space Physics, University of Colorado Boulder, maintained by Makenzie Lystrup. J.E.P. Connerney and Takehiko Satoh were visiting astronomers at the NASA Infrared Telescope Facility, which is operated by the University of Hawaii under Cooperative Agreement no. NNX-08AE38A with the National Aeronautics and Space Administration, Science Mission Directorate, Planetary Astronomy Program. This research was supported by the International Space Science Institute (ISSI) in Bern, through ISSI International Team project 592.

References

Achilleos, N., Miller, S., Tennyson, J., Aylward, A. D., Mueller-Wodarg, I., & Rees, D. (1998). JIM: A time-dependent, three-dimensional model of Jupiter's thermosphere and ionosphere. *Journal of Geophysical Research*, *103*(E9), 20089–20112. https://doi.org/10.1029/98JE00947

Amm, O. (1997). Ionospheric elementary current systems in spherical coordinates and their application. *Journal of Geomagnetism and Geoelectricity*, *49*(7), 947–955. https://doi.org/10.5636/jgg.49.947

Amm, O., & Viljanen, A. (1999). Ionospheric disturbance magnetic field continuation from the ground to the ionosphere using spherical elementary current systems. *Earth, Planets and Space*, *51*(6), 431–440. https://doi.org/10.1186/BF03352247

Badman, S. V., Bonfond, B., Fujimoto, M., Gray, R. L., Kasaba, Y., Kasahara, S., et al. (2016). Weakening of Jupiter's main auroral emission during January 2014. *Geophysical Research Letters*, *43*(3), 988–997. https://doi.org/10.1002/2015GL067366

Baron, R. L., Owen, T., Connerney, J. E. P., Satoh, T., & Harrington, J. (1996). Solar wind control of Jupiter's H^+_3Auroras. *Icarus*, *120*(2), 437–442. https://doi.org/10.1006/icar.1996.0063

Bonfond, B., Grodent, D., Gérard, J. C., Stallard, T., Clarke, J. T., Yoneda, M., et al. (2012). Auroral evidence of Io's control over the magnetosphere of Jupiter. *Geophysical Research Letters*, *39*(1), L01105. https://doi.org/10.1029/2011GL050253

Bonfond, B., Gustin, J., Gérard, J. C., Grodent, D., Radioti, A., Palmaerts, B., et al. (2015). The far-ultraviolet main auroral emission at Jupiter—Part 1: Dawn-dusk brightness asymmetries. *Annales Geophysicae*, *33*(10), 1203–1209. https://doi.org/10.5194/angeo-33-1203-2015

Bonfond, B., Yao, Z., & Grodent, D. (2020). Six pieces of evidence against the corotation enforcement theory to explain the main aurora at Jupiter. *Journal of Geophysical Research: Space Physics*, *125*(11), e28152. https://doi.org/10.1029/2020JA028152

Caldwell, J., Turgeon, B., & Hua, X. M. (1992). Hubble space telescope imaging of the north polar aurora on Jupiter. *Science*, *257*(5076), 1512–1515. https://doi.org/10.1126/science.257.5076.1512

Cavalié, T., Benmahi, B., Hue, V., Moreno, R., Lellouch, E., Fouchet, T., et al. (2021). First direct measurement of auroral and equatorial jets in the stratosphere of Jupiter. *Astronomy and Astrophysics*, *647*, L8. https://doi.org/10.1051/0004-6361/202140330

Chané, E., Saur, J., & Poedts, S. (2013). Modeling Jupiter's magnetosphere: Influence of the internal sources. *Journal of Geophysical Research: Space Physics*, *118*(5), 2157–2172. https://doi.org/10.1002/jgra.50258

Clarke, J. T., Nichols, J. D., Gérard, J. C., Grodent, D., Hansen, K. C., Kurth, W., et al. (2009). Response of Jupiter's and Saturn's auroral activity to the solar wind. *Journal of Geophysical Research*, *114*(A5), A05210. https://doi.org/10.1029/2008JA013694

Connerney, J. E. P., Acuña, M. H., Ness, N. F., & Satoh, T. (1998). New models of Jupiter's magnetic field constrained by the Io flux tube footprint. *Journal of Geophysical Research*, *103*(A6), 11929–11940. https://doi.org/10.1029/97JA03726

Connerney, J. E. P., Kotsiaros, S., Oliversen, R. J., Espley, J. R., Joergensen, J. L., Joergensen, P. S., et al. (2018). A new model of Jupiter's magnetic field from Juno's first nine orbits. *Geophysical Research Letters*, *45*(6), 2590–2596. https://doi.org/10.1002/2018GL077312

Connerney, J. E. P., Satoh, T., & Baron, R. L. (1996). Interpretation of auroral "Lightcurves" with application to Jovian H^+_3Emissions. *Icarus*, *122*(1), 24–35. https://doi.org/10.1006/icar.1996.0107

Connerney, J. E. P., Timmins, S., Oliversen, R. J., Espley, J. R., Joergensen, J. L., Kotsiaros, S., et al. (2022). A new model of Jupiter's magnetic field at the completion of Juno's prime mission. *Journal of Geophysical Research: Planets*, *127*(2), e07055. https://doi.org/10.1029/2021JE007055

Cowley, S. W. H., & Bunce, E. J. (2001). Origin of the main auroral oval in Jupiter's coupled magnetosphere-ionosphere system. *Planetary and Space Science*, *49*(10–11), 1067–1088. https://doi.org/10.1016/S0032-0633(00)00167-7

Cowley, S. W. H., Bunce, E. J., & O'Rourke, J. M. (2004). A simple quantitative model of plasma flows and currents in Saturn's polar ionosphere. *Journal of Geophysical Research*, *109*(A5), A05212. https://doi.org/10.1029/2003JA010375

Coxon, J. C., Chisham, G., Freeman, M. P., Anderson, B. J., & Fear, R. C. (2022). Distributions of Birkeland current density observed by AMPERE are heavy-tailed or long-tailed. *Journal of Geophysical Research: Space Physics*, *127*(2), e2021JA029801. https://doi.org/10.1029/2021JA029801

Coxon, J. C., Milan, S. E., Carter, J. A., Clausen, L. B. N., Anderson, B. J., & Korth, H. (2016). Seasonal and diurnal variations in AMPERE observations of the Birkeland currents compared to modeled results. *Journal of Geophysical Research: Space Physics*, *121*(5), 4027–4040. https://doi.org/10.1002/2015JA022050

Damiano, P. A., Delamere, P. A., Kim, E. H., Johnson, J. R., & Ng, C. S. (2023). Electron energization by inertial Alfvén waves in density depleted flux tubes at Jupiter. *Geophysical Research Letters*, *50*(5), e2022GL102467. https://doi.org/10.1029/2022GL102467

Delamere, P. A., Wilson, R. J., Wing, S., Smith, A. R., Mino, B., Spitler, C., et al. (2024). Signatures of open magnetic flux in Jupiter's dawnside magnetotail. *AGU Advances*, *5*(2), e2023AV001111. https://doi.org/10.1029/2023AV001111

Elsner, R. F., Lugaz, N., Waite, J. H., Cravens, T. E., Gladstone, G. R., Ford, P., et al. (2005). Simultaneous Chandra X ray, Hubble Space Telescope ultraviolet, and Ulysses radio observations of Jupiter's aurora. *Journal of Geophysical Research*, *110*(A1), A01207. https://doi.org/10.1029/2004JA010717

Evans, D. S., Maynard, N. C., Troim, J., Jacobsen, T., & Egeland, A. (1977). Auroral vector electric field and particle comparisons, 2, Electrodynamics of an arc. *Journal of Geophysical Research*, *82*(16), 2235–2249. https://doi.org/10.1029/JA082i016p02235

Fukushima, N. (1976). Generalized theorem for no ground magnetic effect of vertical currents connected with Pedersen currents in the uniform-conductivity ionosphere. *Report of Ionosphere and Space Research in Japan*, *30*(1–2), 35–40.

Gérard, J. C., Gkouvelis, L., Bonfond, B., Grodent, D., Gladstone, G. R., Hue, V., et al. (2020). Spatial distribution of the Pedersen conductance in the Jovian aurora from Juno-UVS spectral images. *Journal of Geophysical Research: Space Physics*, *125*(8), e28142. https://doi.org/10.1029/2020JA028142

Gérard, J. C., Grodent, D., Radioti, A., Bonfond, B., & Clarke, J. T. (2013). Hubble observations of Jupiter's north-south conjugate ultraviolet aurora. *Icarus*, *226*(2), 1559–1567. https://doi.org/10.1016/j.icarus.2013.08.017

Gérard, J. C., Mura, A., Bonfond, B., Gladstone, G. R., Adriani, A., Hue, V., et al. (2018). Concurrent ultraviolet and infrared observations of the north Jovian aurora during Juno's first perijove. *Icarus*, *312*, 145–156. https://doi.org/10.1016/j.icarus.2018.04.020

Greathouse, T., Gladstone, R., Versteeg, M., Hue, V., Kammer, J., Giles, R., et al. (2021). Local time dependence of Jupiter's polar auroral emissions observed by Juno UVS. *Journal of Geophysical Research: Planets*, *126*(12), e06954. https://doi.org/10.1029/2021JE006954

Grodent, D. (2015). A brief review of ultraviolet auroral emissions on giant planets. *Space Science Reviews*, *187*(1–4), 23–50. https://doi.org/10.1007/s11214-014-0052-8

Grodent, D., Bonfond, B., GéRard, J.-C., Radioti, A., Gustin, J., Clarke, J. T., et al. (2008). Auroral evidence of a localized magnetic anomaly in Jupiter's northern hemisphere. *Journal of Geophysical Research*, *113*(A9), A09201. https://doi.org/10.1029/2008JA013185

Hill, T. W. (1979). Inertial limit on corotation. *Journal of Geophysics Research*, *84*(A11), 6554–6558. https://doi.org/10.1029/JA084iA11p06554

Johnson, R. E., Melin, H., Stallard, T. S., Tao, C., Nichols, J. D., & Chowdhury, M. N. (2018). Mapping H_3^+ temperatures in Jupiter's northern auroral ionosphere using VLT-CRIRES. *Journal of Geophysical Research: Space Physics*, *123*(7), 5990–6008. https://doi.org/10.1029/2018JA025511

Juusola, L., Viljanen, A., Partamies, N., Vanhamäki, H., Kellinsalmi, M., & Walker, S. (2023). Three principal components describe the spatiotemporal development of mesoscale ionospheric equivalent currents around substorm onsets. *Annales Geophysicae*, *41*(2), 483–510. https://doi.org/10.5194/angeo-41-483-2023

Kita, H., Fujisawa, S., Tao, C., Kagitani, M., Sakanoi, T., & Kasaba, Y. (2018). Horizontal and vertical structures of Jovian infrared aurora: Observation using Subaru IRCS with adaptive optics. *Icarus*, *313*, 93–106. https://doi.org/10.1016/j.icarus.2018.05.002

Kotsiaros, S., Connerney, J. E. P., Clark, G., Allegrini, F., Gladstone, G. R., Kurth, W. S., et al. (2019). Birkeland currents in Jupiter's magnetosphere observed by the polar-orbiting Juno spacecraft. *Nature Astronomy*, *3*(10), 904–909. https://doi.org/10.1038/s41550-019-0819-7

Krupp, N., Lagg, A., Livi, S., Wilken, B., Woch, J., Roelof, E. C., & Williams, D. J. (2001). Global flows of energetic ions in Jupiter's equatorial plane: First-order approximation. *Journal of Geophysics Research*, *106*(A11), 26017–26032. https://doi.org/10.1029/2000JA900138

Lam, H. A. (1996). *H_3^+ in the Jovian planets* (PhD thesis). University of London, University College London. Retrieved from https://discovery.ucl.ac.uk/id/eprint/10097910/

Laundal, K. M., Gjerloev, J. W., Østgaard, N., Reistad, J. P., Haaland, S., Snekvik, K., et al. (2016). The impact of sunlight on high-latitude equivalent currents. *Journal of Geophysical Research: Space Physics*, *121*(3), 2715–2726. https://doi.org/10.1002/2015JA022236

Mauk, B. H., Clark, G., Gladstone, G. R., Kotsiaros, S., Adriani, A., Allegrini, F., et al. (2020). Energetic particles and acceleration regions over Jupiter's polar cap and main aurora: A broad overview. *Journal of Geophysical Research: Space Physics*, *125*(3), e27699. https://doi.org/10.1029/2019JA027699

Mauk, B. H., Haggerty, D. K., Paranicas, C., Clark, G., Kollmann, P., Rymer, A. M., et al. (2017). Discrete and broadband electron acceleration in Jupiter's powerful aurora. *Nature*, *549*(7670), 66–69. https://doi.org/10.1038/nature23648

Melin, H., Fletcher, L. N., Stallard, T. S., Miller, S., Trafton, L. M., Moore, L., et al. (2019). The H_3^+ ionosphere of Uranus: Decades-long cooling and local-time morphology. *Philosophical Transactions of the Royal Society of London,Series A*, *377*(2154), 20180408. https://doi.org/10.1098/rsta.2018.0408

Moore, L., O'Donoghue, J., Melin, H., Stallard, T., Tao, C., Zieger, B., et al. (2017). Variability of Jupiter's IR H_3^+ aurorae during Juno approach. *Geophysical Research Letters*, *44*(10), 4513–4522. https://doi.org/10.1002/2017GL073156

Nichols, J. D., Badman, S. V., Bunce, E. J., Clarke, J. T., Cowley, S. W. H., Crary, F. J., et al. (2009). Saturn's equinoctial auroras. *Geophysical Research Letters*, *36*(24), L24102. https://doi.org/10.1029/2009GL041491

Nichols, J. D., & Cowley, S. (2004). Magnetosphere-ionosphere coupling currents in Jupiter's middle magnetosphere: Effect of precipitation-induced enhancement of the ionospheric Pedersen conductivity. *Annales Geophysicae*, *22*(5), 1799–1827. https://doi.org/10.5194/angeo-22-1799-2004

Nichols, J. D., & Cowley, S. W. H. (2022). Relation of Jupiter's dawnside main emission intensity to magnetospheric currents during the Juno Mission. *Journal of Geophysical Research: Space Physics*, *127*(1), e30040. https://doi.org/10.1029/2021JA030040

Oliveira, D. M., Weygand, J. M., Coxon, J. C., & Zesta, E. (2024). Substorm-time ground dB/dt variations controlled by interplanetary shock impact angles: A statistical study. *Space Weather*, *22*(3), e2023SW003767. https://doi.org/10.1029/2023SW003767

Radioti, A., GéRard, J. C., Grodent, D., Bonfond, B., Krupp, N., & Woch, J. (2008). Discontinuity in Jupiter's main auroral oval. *Journal of Geophysical Research*, *113*(A1), A01215. https://doi.org/10.1029/2007JA012610

Ray, L. C., Achilleos, N. A., Vogt, M. F., & Yates, J. N. (2014). Local time variations in Jupiter's magnetosphere-ionosphere coupling system. *Journal of Geophysical Research: Space Physics*, *119*(6), 4740–4751. https://doi.org/10.1002/2014JA019941

Rodríguez-Ovalle, P., Fouchet, T., Guerlet, S., Cavalié, T., Hue, V., López-Puertas, M., et al. (2024). Temperature and composition disturbances in the southern auroral region of Jupiter revealed by JWST/MIRI. *Journal of Geophysical Research: Planets*, *129*(6), e2024JE008299. https://doi.org/10.1029/2024JE008299

Rutala, M. J., Clarke, J. T., Vogt, M. F., & Nichols, J. D. (2024). Variation in the Pedersen conductance near Jupiter's main emission Aurora: Comparison of Hubble space telescope and Galileo measurements. *Journal of Geophysical Research: Space Physics*, *129*(3), e2023JA032122. https://doi.org/10.1029/2023JA032122

Salveter, A., Saur, J., Clark, G., & Mauk, B. H. (2022). Jovian auroral electron precipitation budget—A statistical analysis of diffuse, mono-energetic, and broadband auroral electron distributions. *Journal of Geophysical Research: Space Physics*, *127*(8), e30224. https://doi.org/10.1029/2021JA030224

Sinclair, J. A., Greathouse, T. K., Giles, R. S., Antuñano, A., Moses, J. I., Fouchet, T., et al. (2020). Spatial variations in the altitude of the CH_4 homopause at Jupiter's mid-to-high latitudes, as constrained from IRTF-TEXES spectra. *Planetary Science Journal*, *1*(3), 85. https://doi.org/10.3847/PSJ/abc887

Stallard, T. (2018). The magnetospheres of the outer planets infrared data archive: IRTF NSFCAM 1995–2000 [Dataset]. *Harvard Dataverse*. https://doi.org/10.7910/DVN/KVQWNJ

Stallard, T. (2025). Jupiter's varying auroral emission 1: Plot data and code [Collection]. *Harvard Dataverse*. https://doi.org/10.7910/DVN/QKWEJB

Stallard, T., Miller, S., Millward, G., & Joseph, R. D. (2002). On the dynamics of the Jovian ionosphere and thermosphere. II. The measurement of H_3^+ vibrational temperature, column density, and total emission. *Icarus*, *156*(2), 498–514. https://doi.org/10.1006/icar.2001.6793

Stallard, T. S., Burrell, A. G., Melin, H., Fletcher, L. N., Miller, S., Moore, L., et al. (2018). Identification of Jupiter's magnetic equator through H_3^+ ionospheric emission. *Nature Astronomy*, *2*(10), 773–777. https://doi.org/10.1038/s41550-018-0523-z

Stallard, T. S., Clarke, J. T., Melin, H., Miller, S., Nichols, J. D., O'Donoghue, J., et al. (2016). Stability within Jupiter's polar auroral "Swirl region" over moderate timescales. *Icarus*, *268*, 145–155. https://doi.org/10.1016/j.icarus.2015.12.044

Strobel, D. F., & Atreya, S. K. (1983). Physics of the Jovian magnetosphere. 2. Ionosphere. In *Physics of the Jovian magnetosphere* (pp. 51–67). Cambridge University Press. https://doi.org/10.1017/CBO9780511564574.004

Tao, C., Badman, S. V., & Fujimoto, M. (2011). UV and IR auroral emission model for the outer planets: Jupiter and Saturn comparison. *Icarus*, *213*(2), 581–592. https://doi.org/10.1016/j.icarus.2011.04.001

Tao, C., Fujiwara, H., & Kasaba, Y. (2009). Neutral wind control of the Jovian magnetosphere-ionosphere current system. *Journal of Geophysical Research*, *114*(A8), A08307. https://doi.org/10.1029/2008JA013966

Tao, C., Fujiwara, H., & Kasaba, Y. (2010). Jovian magnetosphere-ionosphere current system characterized by diurnal variation of ionospheric conductance. *Planetary and Space Science*, *58*(3), 351–364. https://doi.org/10.1016/j.pss.2009.10.005

Tsubota, T. K., Wong, M. H., Stallard, T., Zhang, X., & Simon, A. A. (2024). UV-dark polar ovals on Jupiter as tracers of magnetosphere-atmosphere connections. *Nature Astronomy*, *9*(2), 221–229. https://doi.org/10.1038/s41550-024-02419-0

Vogt, M. F., Kivelson, M. G., Khurana, K. K., Walker, R. J., Bonfond, B., Grodent, D., & Radioti, A. (2011). Improved mapping of Jupiter's auroral features to magnetospheric sources. *Journal of Geophysical Research*, *116*(A3), A03220. https://doi.org/10.1029/2010JA016148

Wang, J.-Z., Bagenal, F., Wilson, R. J., Nerney, E., Ebert, R. W., Valek, P. W., et al. (2024). Dawn-dusk asymmetry of plasma flow in Jupiter's middle magnetosphere observed by Juno. *Geophysical Research Letters*, *51*(19), e2024GL110209. https://doi.org/10.1029/2024GL110209

Wang, R., Stallard, T. S., Melin, H., Baines, K. H., Achilleos, N., Rymer, A. M., et al. (2023). Asymmetric ionospheric jets in Jupiter's aurora. *Journal of Geophysical Research: Space Physics*, *128*(12), e2023JA031861. https://doi.org/10.1029/2023JA031861

Watanabe, H., Kita, H., Tao, C., Kagitani, M., Sakanoi, T., & Kasaba, Y. (2018). Pulsation characteristics of Jovian infrared northern aurora observed by the Subaru IRCS with adaptive optics. *Geophysical Research Letters*, *45*(21), 11547–11554. https://doi.org/10.1029/2018GL079411

Weygand, J. M., Hartinger, M. D., Strangeway, R. J., Welling, D. T., Kim, H., Matzka, J., & Clauer, C. R. (2023). Interhemispheric asymmetry due to IMF By within the cusp spherical elementary currents. *Journal of Geophysical Research: Space Physics*, *128*(6), e2023JA031430. https://doi.org/10.1029/2023JA031430

Workayehu, A. B., Vanhamäki, H., & Aikio, A. T. (2019). Field-aligned and horizontal currents in the Northern and Southern Hemispheres from the Swarm Satellite. *Journal of Geophysical Research: Space Physics*, *124*(8), 7231–7246. https://doi.org/10.1029/2019JA026835

Workayehu, A. B., Vanhamäki, H., & Aikio, A. T. (2020). Seasonal effect on hemispheric asymmetry in ionospheric horizontal and field-aligned currents. *Journal of Geophysical Research: Space Physics*, *125*(10), e28051. https://doi.org/10.1029/2020JA028051

Workayehu, A. B., Vanhamäki, H., Aikio, A. T., & Shepherd, S. G. (2021). Effect of interplanetary magnetic field on hemispheric asymmetry in ionospheric horizontal and field-aligned currents during different seasons. *Journal of Geophysical Research: Space Physics*, *126*(10), e29475. https://doi.org/10.1029/2021JA029475

Xiong, C., Stolle, C., Alken, P., & Rauberg, J. (2020). Relationship between large-scale ionospheric field-aligned currents and electron/ion precipitations: DMSP observations. *Earth Planets and Space*, *72*(1), 147. https://doi.org/10.1186/s40623-020-01286-z

Zhang, B., Delamere, P. A., Yao, Z., Bonfond, B., Lin, D., Sorathia, K. A., et al. (2021). How Jupiter's unusual magnetospheric topology structures its aurora. *Science Advances*, *7*(15), eabd1204. https://doi.org/10.1126/sciadv.abd1204